Red Blood Cell Surface Segmentation Based on Shape Reconstruction and Statistics Feature Extraction

Ruihu Wang
Department of Science and Technology, Chongqing University of Arts and Sciences, Chongqing, China
Email: ruihu.wang@yahoo.com.cn

***Abstract*—There is considerable evidence demonstrating that erythrocyte deformability is playing an important role in the filerability of blood and consequently in the pathology of a variety of blood-related diseases. The shape of red blood cell is also a determining factor for its deformability and filerability. The original input red blood cell image we are aiming to deal with is captured by Scanned Electronic Microscope (SEM). We map the intensity level image into a 3-D depth through Shape from Shading (SFS) first to get the height field of each pixel, then each cell on top level is extracted from the whole image by means of region growing algorithm based on boundary contour tracing, which are used for feature extraction and statistics computation. The experimental result shows that this approach is easily to implement and promising.**

***Index Terms*—red blood cell, contour tracing, shape reconstruction, surface segmentation**

I. INTRODUCTION

Erythrocytes (Red Blood Cells) are produced in the bone marrow, and (after about 120 days) are degraded in the spleen and liver. They are the most common (>99%) blood cells and of nucleus and organelles. It is common knowledge that erythrocytes are important to maintain human's normal physiology function. They deliver Oxygen into various organs and transport carbon dioxide produced by cell metabolism back to lung. Furthermore, there is considerable evidence authenticating that erythrocyte deformability is an important determinant in the filerability of blood and consequently in the pathology of a variety of blood-related diseases. In addition, the shape of red blood cell is also a determining factor for its deformability and filerability. In a matter of fact, Myalgic Encephalomyelitis (ME) and Multiple Sclerosis （MS） [85-90] arise from the degradation of erythorocyte deformability in pathology research. Therefore when clinic diagonosing, the shape analyzing of erythrocyte is helpful for physician to discriminate what kind of state of an illness the patient suffered.

The most mainly used method for analyzing erythrocytes deformability is computing the shape distribution of various kinds of cells in a red blood cell image. Due to the variability of erythrocyte shape, it is not appropriate to employ traditional methods here like 2D image processing technique any more. The difficulty of adopting the existing results of former studies from the laboratory to clinical diagnosis or measuring the effectiveness of treatment is mostly on account of the large amount of tedious work required to measure the distribution of different erythrocyte cells from a sample [4]. It is time-consuming and low efficiency when using traditonal artificial analyzing, which rely a lot on human's intuitive impression estimation. Accordingly, the erythrocytes' deformability and shape information should be taken into consideration to build up an automatic processing system.

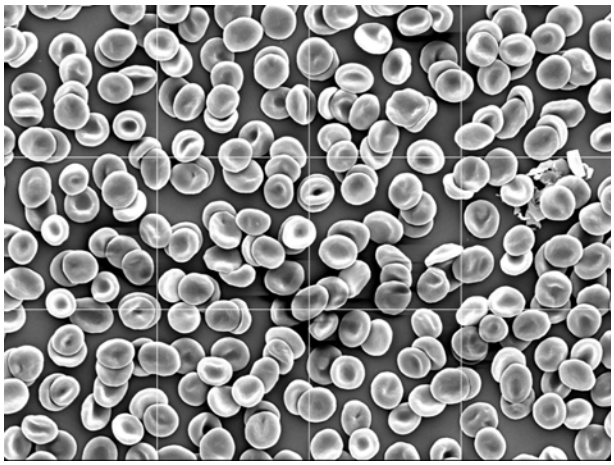

Figure 1. A typical SEM image of red blood cells

Figure 1 shows a typical example of such kind of Red Blood Cell images captured by SEM with which we are going to deal. They were obtained at 600 times magnification using a scanned electron microscope. As shown in Figure 1, there are some outstanding characteristics about this image which make our problem be significant and challenging. On the one hand, the image represents very highly good quality with varied shading illuminated by light source. On the other hand, some light grid lines is superimposed in the image. The grid lines were added for the sake of manual counting. In addition, those cells' shape takes on lots of irregular deformation, which is the primary problem we have to solve to segment effectively. As we well known, image segmentation is the bridge to classification properly. We aimed to develop a satisfied algorithm to classify the Red Blood Cells into different groups accurately. And also we

doi:10.4304/jcp.8.4.1083-1089

believed that conventional segmentation methods based on gray value could be unsuitable to this case. In this paper we proposed a new strategy to segment RBC image according to surface feature extraction. At first, we have to estimate the distribution of erythrocyte shapes from scanned electron microscope. Then each cell's three dimension shape was reconstructed as 3D height field using Shape from Shading technique. Lastly we implement multi-scale surface fitting segmentation algorithm to partition the cells based on the depth data acquired in the previous procedures.

The detailed information of each Section is described as following. As there are lots of overlapped red blood cells in the original image, we only interested in the top level cells with regarding to statistics feature. In Section II, each cell is extracted individually from the whole image by using region growing algorithm which is based on boundary contour tracing. The segmentation algorithm consists of two main procedure, contour tracing and region growing respectively.

Due to high quality of red blood cell image captured by SEM, which present clear shading information, we proposed a three dimension reconstruction approach for cell surface shape based on seeking a solution for the reflection equation solving using linear approximation. In Section III, we made an appropriate assumption that the cell surface reflection is Lambertian model, linear approximation difference based on Taylor expansion is employed to solve the Image Iradiance partial diffenrential Equation (IRE). The reconstructed three dimension height field can be viewed as reange image which is to be input for cell image surface segmentation.

An adaptive curved surface fitting and curvature computation methods for irregular cell shape with multi-deformation are put forward in Section IV. After height field reconstructed with Shape-from-Shading technique, the three dimensional data points are used for surface fitting based on least square method. The fitting points are selected in terms of depth root mean square error (RMSE) threshold pre-set. As we well known, the surface type can be expressed by the sigh of Gaussian curvature and mean curvature. We adopt bi-variate polynomials functions set to realize the surface fitting from which the surface patches can be segmented successfully.

II. System Architecture

As shown in Figure 1, there existed some bright grid lines superimposed on the original image, which have some side effects on the subsequent work. As mentioned before, the images show perfect quality other than this lines, which is used to count and classification manually. The system we developed here is to relieve human from exhausted hand work and run automatically. Additionally, in terms of the shading information being critical in our case, we regard the lines as noise and we have to remove them before recovering the 3D shape from gray tone image. As shown in Fig 2, the first procedure of the whole system is image preprocessing which results in the elimination of those white grid lines.

As time consumption is sensitive during RBCs classification, we make use of median filter to get rid of the grid lines. The median filter is a smoothing technique that causes minimal edge blurring, which involves replacing the pixel value at each point in an image by the median of the pixel values in a neighborhood about the point.

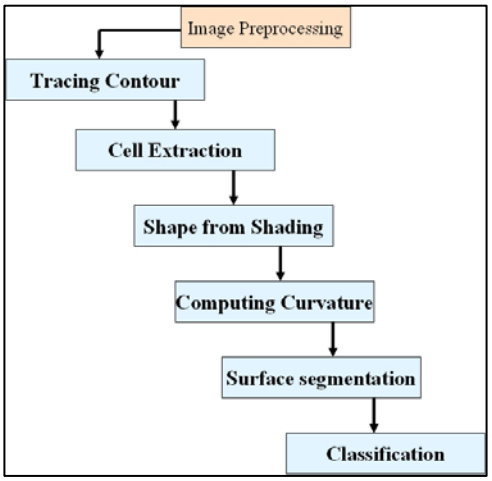

Figure 2. System architecture

Definition 1 Let *S* denotes the neighborhood around the pixel point coordinated with (x_0, y_0) and $(x, y) \in S$. The gray level value of (x, y) is represented by $f(x, y)$ and $|S|$ is the pixel number in set *S*. The smoothing operation on (x_0, y_0) can be formulated as:

$$f'(x_0, y_0) = \left[\underset{(x,y)\in S}{Sort} \; f(x, y) \right]_{\frac{|S|+1}{2}}$$

The denoised image after median filtering directly on the whole image in which the lines are removed successfully, However, the edges of cell image have been blurred and brightness changed at the same time. Consequently the issue of inaccuracy would arise from the change, because the recovered shape is relied on the irradiance mostly. Fortunately we can detect the exact positions where those lines are in by horizontal and vertical projection using

$$\sum_{i \oplus j} Q(i, j)$$

respectively. Where $Q(i,j)$ only represents those pixels whose gray value is approximately equal to the pixels in those white grid lines. Experimental result show that when determining the exact positions of vertical lines, the points located in the range of $i \in [253, 259]$ or $[509, 517]$ have to be considered only. And those points whose *j* coordinate is in the range of $j \in [253, 259]$ or $[509, 515]$ or $[765, 771]$ have to be dealt with when impose median filtering locally.

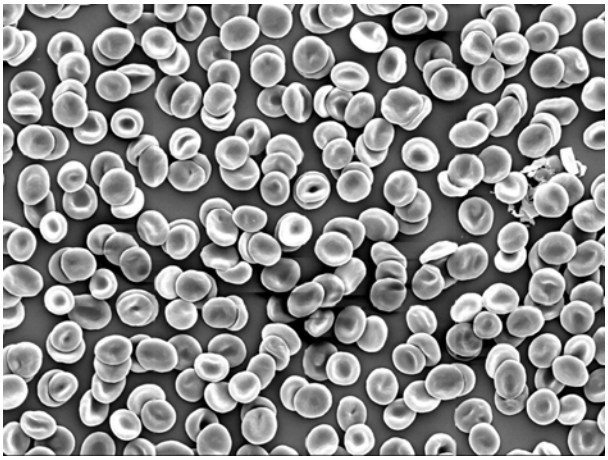

Figure 3. Preprocessing of red blood cell image using median filtering locally(gridline removing)

III. TRACING CONTOUR AND CELL EXTRACTION

A. Guided Contour Tracing

Vromen and McCane [5] proposed a method named contour tracing based approach to the problem of finding the boundary of red blood cells in a Scanned Electron Microscope image automatically. As shown in above Figure 1, there are considerable overlapped cells. We are just only interested in estimating the distribution of different erythrocyte shapes from SEM image rather than the accurate counting number. So it makes sense to assume that the distribution of overlapped cells is identical to the overall distribution. Consequently only those top level cells are needed to be detected and recognized. At the very beginning, the most possible direction are chosen by taking the prior information of tracing into account so far.

They formulated the tracing problem in a simple Bayesian tracking framework. Suppose that there are n contours in a image,

Let

$$\{C_i\}, i = 1, \cdots, n$$

denotes the set of all unobscured contours, and for each $C_j \in \{C_i\}, j = 1, \cdots, n$, $C_j = x_{0:N_j}$. It means the j^{th} contour consists of a set of image points, marked by $x_0, x_1, \cdots, x_{N_j}$ respectively. In the set of points, x_0 is a given starting point. They concluded the tracing problem was to build a closed contour C_j iteratively until a loop was achieved.

In each decision stage, the next point x_{k+1} should maximizes,

$$\arg\max_{x_{k+1}} p(x_{k+1} \mid x_{0:k}, G) = \frac{p(G \mid x_{0:k+1}) p(x_{k+1} \mid x_{0:k})}{p(x_{0:k} \mid G)} \tag{3.1}$$

where G was gradient map which was calculated using a simple finite difference approximation.

In their method, after several simplifying assumption adopted, the problem was transformed to determine the direction which was to choose the next step according to the current direction of motion. Ultimately, a parameter θ was needed to be chosen so as to maximize:

$$p(\theta \mid x_{0:k}, G) \propto p(G \mid \theta) p(\theta \mid x_{(k-n_l):k}) \tag{3.2}$$

In our experiment, all of the points' position information within a contour was stored as different attributes in an XML file. It also contained the locus of each point on the boundary as following.

```
<?xml version="1.0" encoding="UTF-8" ?>
<contour_trace>
  <image src="mri423.png" />
  <contour center_x="31.3996" center_y="408.217"
  radius_x="28.582" adius_y="24.0934" size="166">
   <point x="35.9251" y="379.38" />
     <point x="36.8389" y="379.786" />
     <point x="37.7858" y="380.108" />
     <point x="38.7157" y="380.475" />
     <point x="39.6394" y="380.858" />
     <point x="40.5593" y="381.25" />
     ……
  </contour>
```

B. Cell Extraction Individually

According to the extracted cell contours information, we can grow each cell starting at center point regionally to get the entire cell image. The result image of region growing subject to contour boundary is shown in Figure 4. After growing regionally we got the number of pixels which make the whole image and their gray level value.

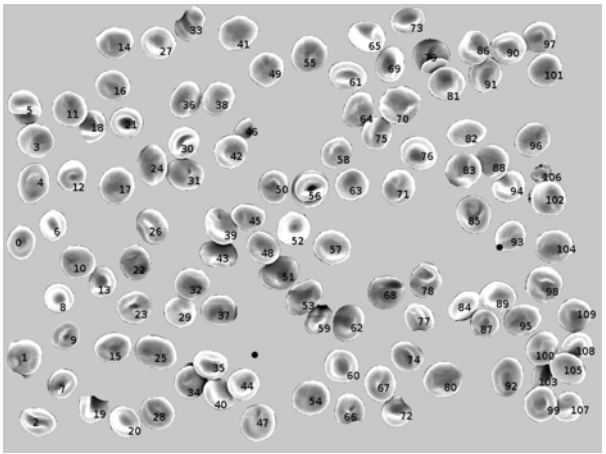

Figure 4. Extracted Cell Image

IV. SHAPE RECONSTRUCTION

A. Image Radiance Equation

The radiance of surface patch is dependent on gradient, light source location and reflectance property. The gray level of a pixel in the image is determined by light direction and normal vector, as shown in Fig.5.

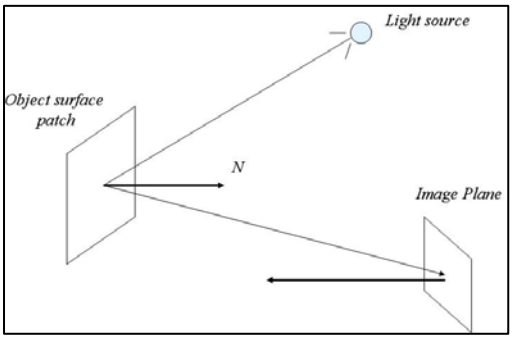

Figure 5. Illumination Model

In Fig.6, Φ denotes the radiant energy or flux in a volume V . Radiance (*L*) is the flux that leaves a surface, per unit projected area of the surface, per unit solid angle of direction. Irradiance is the flux per unit area that arrives at
a surface, denoted by *E*.

$$d\Phi = E\, dA \tag{4.1}$$

holds true.

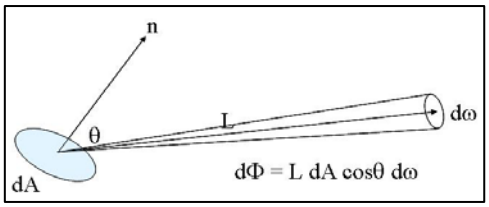

Figure 6. Radiance and Irradiance

There are two kinds of reflection model: Specular model and Lambertian model respectively. Regarding to the properties of the cell surface, we assumed that shading is formed by Lambertian reflection function. And

$$I_{diffuse} = I_d K_d \cos\theta$$

(4.2)

where $I_{diffuse}$ represents diffuse reflection light intensity of
a point. I_d is point light source, and $K_d (0 < K_d < 1)$
denotes reflection attributes. θ is a intersection angle between the reflection light and the normal *N* on the point.

Image Radiance Equation (*IRE*) indicates the relationship between reflection function and image radiance. The recovered shape can be represented by depth map Z, normal n_x, n_y, n_z ,or surface gradient (p,q) . The radiance of surface patch depends on gradient, light source location and reflectance property. The gray level of a pixel in the image is determined by light direction and normal vector, assumed Lambertian model, which can be denoted by **IRE**:

$$E(x,y) = R(p,q) = \frac{1 + pp_s + qq_s}{\sqrt{1+p^2+q^2}\sqrt{1+p_s^2+q_s^2}}$$

(4.3)

where $E(x,y)$ is a gray level at pixel (x,y),

$$p = \frac{\partial z}{\partial x}$$

and

$$q = \frac{\partial z}{\partial y},$$

$(p_s, q_s, 1)$ is the illumination direction.

B. Linear Approximation

In [14], the authors believed that the linearity of the reflectance map in the depth *Z*, instead of *p* and *q* , is more appropriate in some cases. They presented a method for computing depth from a single shaded image by employing the discrete approximations for *p* and *q* using finite differences, and linearly approximates the reflectance in *Z*(*x*,*y*). It gave good results for the spherical surface and can be applied to any reflectance function.

By approximating the *p* and *q* discretely, we get

$$p = \frac{\partial z}{\partial x} = Z(x,y) - Z(x-1,y)$$

(4.4)

$$q = \frac{\partial z}{\partial y} = Z(x,y) - Z(x,y-1)$$

(4.5)

According to (4.3)-(4.5) , the reflection function can be rewritten as:

$$E(x,y) = R(p,q) = R(z(x,y), z(x-1,y), z(x,y-1))$$

And

$$0 = E(x,y) - R\left(Z(x,y) - Z(x-1,y), Z(x,y) - Z(x,y-1)\right)$$
$$= f\left(E(x,y), Z(x,y), Z(x-1,y), Z(x,y-1)\right)$$

After ***Taylor Expansion*** and ***Jacobi Iteration***, the above equation can be represented as:

$$0 = f\left(Z(x,y)\right) =$$
$$f\left(Z^{n-1}(x,y)\right) + \left(Z(x,y) - Z^{n-1}(x,y)\right)\frac{d}{dZ(x,y)} f\left(Z^{n-1}(x,y)\right) \tag{4.6}$$

And,

$$Z^n(x,y) = Z^{n-1}(x,y) + \frac{-f\left(Z^{n-1}(x,y)\right)}{\frac{d}{dZ(x,y)} f\left(Z^{n-1}(x,y)\right)} \tag{4.7}$$

As mentioned previously, the reflection function inverses to *Lambertian* model under the condition of SEM imaging, which can be described as below:

$$R(p,q)=\frac{\sqrt{1+p^2+q^2}\sqrt{1+p_s^2+q_s^2}}{1+pp_s+qq_s}$$

which can be used to compute the second term of the right hand in (4.7):

$$Z^n(x,y)=Z^{n-1}(x,y)+\frac{f\left(Z^{n-1}(x,y)\right)\cdot\left(1+pp_s+qq_s\right)^2\cdot\sqrt{1+p^2+q^2}}{\left(\left(1+pp_s+qq_s\right)(p+q)-\left(1+p^2+q^2\right)(p_s+q_s)\right)\cdot\sqrt{1+p_s^2+q_s^2}}$$

V. Surface Feature Extraction

The intensity image has been transformed into range image after surface reconstruction using shape from shading technique. Those discrete 3D data points cannot be used for computing surface feature directly. In order to obtain the surface statistics feature, surface fitting has to be performed firstly.

A. Gaussian Curvature and Mean Curvature

A curved surface denoted by $z=f(x,y)$ can be represented as $p(x,y)=(x,y,z)=(x,y,f(x,y))$ implicitly.

Let

$$u=\frac{\partial f(x,y)}{\partial x},\qquad v=\frac{\partial f(x,y)}{\partial y}$$

$$E=1+u^2\qquad F=uv\qquad G=1+v^2$$

$$L=\frac{\frac{\partial u}{\partial x}}{\sqrt{1+u^2+v_2}}\qquad N=\frac{\frac{\partial v}{\partial y}}{\sqrt{1+u^2+v_2}}$$

$$M=\frac{\frac{\partial u}{\partial y}}{\sqrt{1+u^2+v_2}}=\frac{\frac{\partial v}{\partial x}}{\sqrt{1+u^2+v_2}}$$

Then Gaussian Curvature is

$$K=\frac{LN-M^2}{EG-F^2}.$$

And Mean Curvature is

$$H=\frac{EN-2FM+GL}{2(EG-F^2)}$$

Both of these two curvatures can be calculated by local convolution [15]. The Gaussian curvature and mean curvature in a digital surface can be denoted as:

$$H=\frac{(1+g_v^2)g_{uu}+(1+g_u^2)g_{vv}-2g_ug_vg_{uv}}{2(\sqrt{1+g_u^2+g_v^2})^3}$$

$$K=\frac{g_{uu}g_{vv}-g_{uv}^2}{(1+g_u^2+g_v^2)^2}$$

The surface type of each data point on a scene object can be designated by the signs of mean curvature and Gaussian curvature uniquely as:

$$T=1+3(1+3\,\mathrm{sgn}_{\varepsilon_H}(H))+(1-\mathrm{sgn}_{\varepsilon_K}(K))$$

In our experiment we choose

$$\begin{cases}\varepsilon_H=0.0015\\ \varepsilon_K=0.03\end{cases}$$

as the mean curvature threshold and Gaussian curvature separately. In Fig.7, the darker region denote flat surface, and then pit, the lighter is valley.

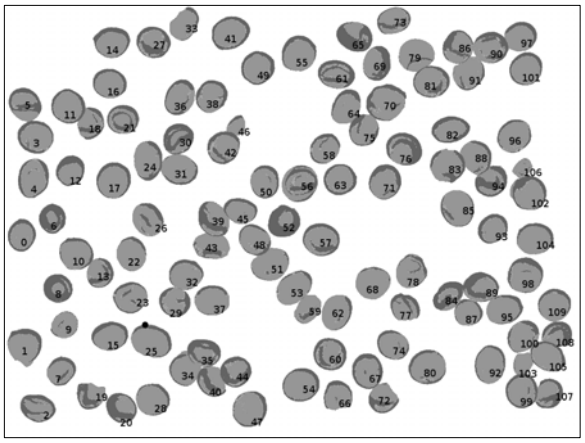

Figure 7. Surface Type Label Image

B. Surface Type Based Image Segmentation

The fundamental formulation of region based image segmentation is defined as [4]:

(1) $U_{i=1}^{n}R_i=R$

(2) R_i is a connected region, $i=1,2,\cdots,n$

(3) $R_i\cap R_j=\Phi,\ for\ \forall(i,j), i\neq j$

(4) $P(R_i)=TRUE, i=1,2,\cdots,n$

(5) $P(R_i\cup R_j)=FALSE$, R_i is adjacent to R_j

where $P(R_i)$ is a uniformity predicate defined on groups of connected pixels. R_i was grown regionally via 8-connected neighborhood. All the points in region R_i satisfy the same surface function. Different regions meet different surface fitting function.

The Root Mean Square Error (RMSE)

$$\sigma_{S_N}^2=\frac{1}{N}\sum_{(x,y)\in S_N}(z_{ij}-\Phi_{\bar{a}}(x,y))^2,$$

between the fitted value and original depth is subject to the range preset by a threshold.

Surface Fitting Algorithm

STEP 1. Initialization

1.1 estimate the noise variance:

$$\sigma_{img}^2=E\left(\sigma_{W_3}^2\right)=\frac{1}{N_{\text{int}}}\sum_{l=1}^{N_{\text{int}}}\left(\sum_{p\in(R_l-\partial R_l)}\sigma_{W_3}^2(p)\right)$$

$$\sigma^2_{W_3}(p)=\frac{1}{9}\sum_{(i,j)\in W_3}(z_{ij}-(a_{00}+a_{10}i+a_{01}j))^2$$

where ∂R represents the boundary of the region *R*, N_{int} is the total number of surface interior pixels contributing to the sum, and $\sigma_{W_3}(p)$ is the root-mean-square-error of the least-squares planar surface fit (a_{00},a_{10},a_{01}) in the 3×3 window W_3 around the pixel p.

1.2 computing mean and Gaussian curvature through separable convolution;

1.3 compute surface type label image and find all connected components of each surface type label image;

1.4 Extract seed region through erosion (contraction):

For each ON pixel in the input binary image, test each of the eight neighbors of that pixel in the input image. If any neighbor is OFF, turn that pixel OFF in the input binary image. Pixels that are OFF in the input binary image remain OFF in the output binary image.

2. Iterative variable order surface fitting

2.1 Perform surface fit from the lowest order, if it is OK using RMS error and region test;

2.2 Then goto 3

2.3 Else increase the order and fit again

2.4 if order > 4, then return

3. Region Growing

3.1 Find the new region consisting of compatible connected neighboring pixels;

C. Experimental result

In our experiment, we define the RMS fit error as $\varepsilon=\omega\sigma_{img}$, where σ_{img} means noise variance, and

$$\hat{z}(p)=\hat{f}(m^k,\vec{a}_l,x(p),y(p))$$

is compared with

$$z(p)=\tilde{g}(x(p),y(p))$$

to see if the pixel *p* is compatible with the approximating surface function. If the magnitude of the difference between the function value and the digital surface value is less than the allowed tolerance value, denoted by $\omega_0\cdot\varepsilon_l^k$, then the pixel *p* is added to the set of compatible pixels, denoted by $C(m_k,\vec{a}_l^k,\varepsilon_l^k)$, which are compatible with the surface fit to the region $\hat{R}_l^k$. Otherwise, the pixel is incompatible and discarded. The result of this process is the compatible pixel list:

$C(m_k,\vec{a}_l^k,\varepsilon_l^k)=p\in I:\left|\hat{z}(p)-z(p)\right|\le\omega_0\varepsilon_l^k$.

We choose $\omega_l=4.5$ and $\omega_0=8$ experimentally.

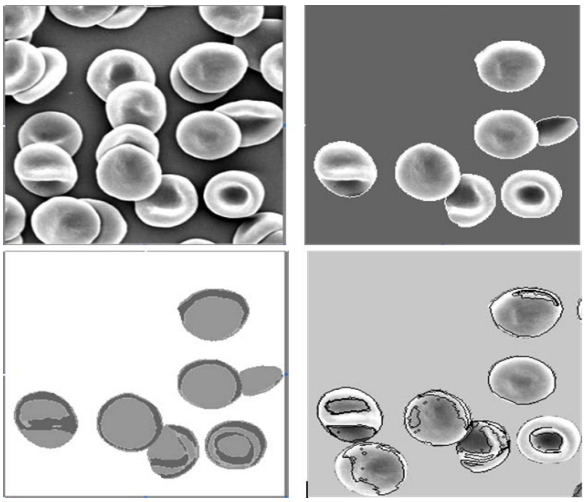

Figure 8. Surface Segmentation Through Fitting

Tab.1 shows the cell distribution in terms of different surface type counting. Fig.9-Fig.11 show three typical type of cells which are with the same surface type distribution.

TABLE I. SURFACE TYPE STATISTICS DISTRIBUTION

Type	Flat	Pit	Valley	Cells Number
1	1	1	0	0,1,2,4,6,8,10,11,12,14,16,17,20,22,24,25,28,29,31,32,33,36,37,38,41,43,44,45,46,47,49,50,51,52,53,55,57,59,62,63,64,65,66,67,68,69,72,75,77,80,82,83,87,90,91,93,95,98,99,101,104,105,108,109(63)
2	1	2	0	5,13,19,27,30,35,39,40,61,79,84,86,89,102,107(15)
3	2	1	0	7,26,34,54,58,70,71,74,85,96,100(11)
4	0	1	0	9,15,31,92,97,103,106(7)
5	3	3	0	18(1)
6	2	2	1	42,56,60(3)
7	3	1	0	23(1)
8	2	2	0	21,73,78,88(4)
9	1	1	1	3,81(2)
10	2	1	1	48(1)
11	1	2	1	76,94(2)

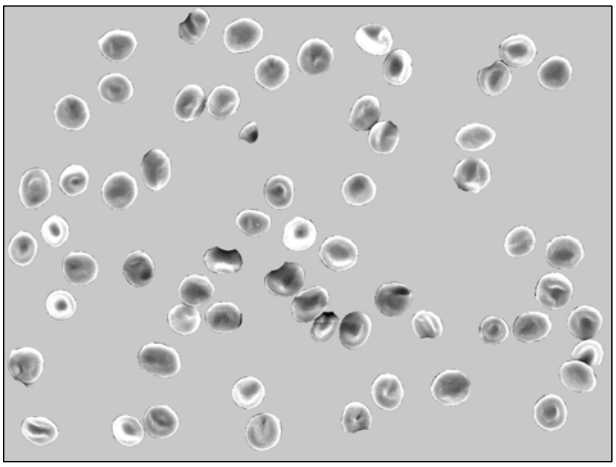

Figure 9. cells with the same surface type distribution (1)

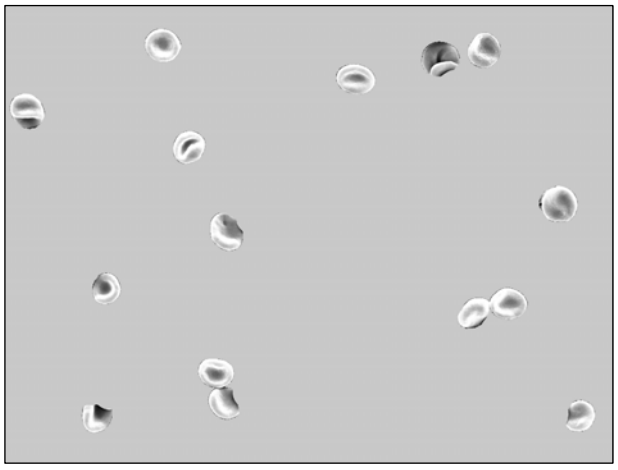

Figure 10. cells with the same surface type distribution (2)

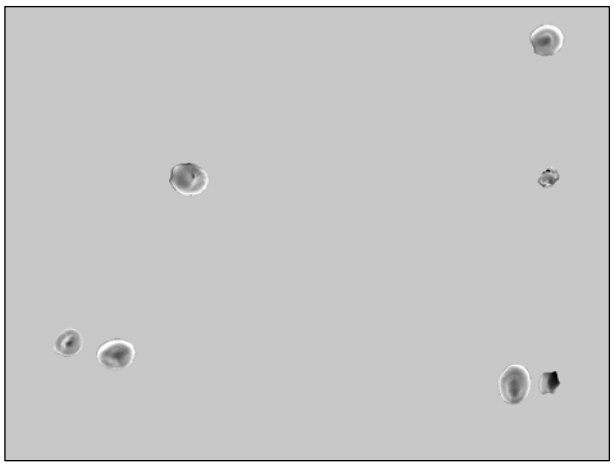

Figure 11. cells with the same surface type distribution (3)

VI. CONCLUSION AND FUTURE WORK

This paper is about how to reconstruct the 3D shape of Red Blood Cell from gray tone images using Scanned Electronic Microscope based on Shape from Shading technique, as well combined with linear approximation. The result of cell surface shape is given by height field. Our algorithm can be trivially transformed to various different kinds of reflection model. The distribution of count number of each surface type in every cell can present some useful information for classifying correctly, which will be trained as input data. In the end, we aim to construct a classifier by means of cascaded SVMs architecture to recognize the red blood cell is normal or not.

ACKNOWLEDGMENT

This work is sponsored by the Excellent Science and Technology Program for Overseas Studying Talents of Chongqing Municipal Human Resources and Social Security Bureau (09958023).

REFERENCES

[1] Ray F.Egerton, Physical Principes of Eletron Miscroscopy, Springer, 2005.

[2] Emmanuel Prados,Olivier Faugeras, Shape from Shading. Handbook of Mathematical Models in Computer Vision, Springer, 2006.

[3] John C.Russ, The image processing handbook, CRC Press, 1992..

[4] Rafael C.Gonzalez,Richard E.Woods,Steven L.Eddins Digital Image Processing, Pearson Education North Asia Limited, 2005..

[5] Joost Vromen,Brendan McCane. Red blood cell segmentation from SEM Image. Image and Vision,New Zealand,2009.

[6] Berthold K.P.Horn,Michael J.Brooks, The variational Approach to Shape from Shading, Image and Vision Computing Computer Vision, Graphics,and Image Processing.33 (1986) 174-208..

[7] Ruo Zhang,Shape from Shading:A survey. IEEE transactions on pattern analysis and machine intelligence,21,690-706.

[8] Emmanuel Prados,Fabio Camilli,Olivier Faugeras. A unifying and rigorous Shape From Shading method adapted to realistic data and applications. Journal of Mathematical Imaging and Vision, 25(2006),307-328

[9] Ariel Tankus,Nir Sochen,Yehezkel Yeshurun. Perspective Shape-from-Shading by Fasting Marching,CVPR 2004,27,143-149.

[10] Ariel Tankus,Nir Sochen,Yehezkel Yeshurun. A New Perspective [on] Shape-from-Shading. ICCV 003.Vol 2. 862:869

[11] Ariel Tankus,Nir Sochen,Yehezkel Yeshurun. Reconstruction of Medical Images by Perspective Shape from Shading. ICPR 2004. Volume.3. 778:781

[12] Koichiro EGUCHI,Takayuki OKATANI, Shape Reconstruction from an Endoscope Image by Shape-from-Shading Technique for a Point Light Source at the Projection Center, Proceeding of the 1996 Workshop on Mathematical Methods in Biomedical Image Analysis,1996 IEEE.

[13] A.G.Jones,C.J.Taylor, Robust Shape from shading. Image and Vision Computing, 12(1994), 411-421.

[14] Ping-Sing Tsai and Mubarak Shah. Shape From Shading Using Linear Approximation, IVC, Volume 12,No,8, 487:498

[15] Paul J.Besl,Ramesh C.Jain. it Surface in Range Image Understanding, Springer-Verlag New York Inc. 1988.

[16] Paul J. Besl, Ramesh C. Jain. Segmentation Through Variable-Order Surface Fitting. IEEE Transactions on Pattern Analysis and Machine Intelligence. Vol.10,No.2:167-192,1988.

[17] S. Bakshi, Y. Yang. Shape from shading for non-lambertain surfaces. In ICIP,94, volume 94, pages 130-134, 1994

[18] K.Lee, C,Kuo. Shape from shading with a generalized reflectance map model. CVIU, 67(2):143-160, 1997

[19] H.Ragheb, E.Hancock. A probabilistic framework for specular shape –from-shading. SIAM J. of Numerical Analysis, 29(3):867-884, 199